Talanta 211 (2020) 120729

Contents lists available at ScienceDirect

Talanta

journal homepage: www.elsevier.com/locate/talanta

Small size nanoparticles—Co_3O_4 based lateral flow immunoassay biosensor for highly sensitive and rapid detection of furazolidone

Lihong Su, Lulu Wang, Xiaolin Yao, Xuechi Yin, Han Zhang, Man Zhao, Sijie Liu, Zonghan Wang, Jianlong Wang, Daohong Zhang*

College of Food Science and Engineering, Northwest A&F University, Yangling, 712100, Shaanxi, China

ARTICLE INFO

Keywords:
Lateral flow immunoassay
Co_3O_4 nanoparticles
Furazolidone
Rapid detection

ABSTRACT

Lateral flow immunoassay (LFIA) biosensor is a paper-based tool and widely utilized in various fields. Here, we developed a novel LFIA biosensor by introducing Co_3O_4 nanoparticles (NPs) as signal labels for highly sensitive detection of 3-amino-2-oxazolidinone (AOZ), a metabolite of furazolidone. The characteristic brown color of Co_3O_4 NPs enabled AOZ to be visually detected by the LFIA. Significantly, the size of Co_3O_4 NPs is relatively small compared with most of other signal labels, which could remarkably reduce steric hindrance, increase immunoreaction probability and shorten the analysis time. Under optimal conditions, the novel Co_3O_4 NPs-LFIA could possess high sensitivity for the detection of AOZ with a detection limit of 0.4 ng mL^{-1} by naked eyes, which was at least 3-fold improved than that of the conventional gold nanoparticles (GNPs) based LFIA. Moreover, the detection could be achieved within 6 min and without cross-reactions with other analogue small molecules. Taking merits of convenience, rapid and sensitivity, the proposed Co_3O_4 NPs-LFIA may be readily adapted for the detection of other small molecules.

1. Introduction

The Lateral flow immunoassay (LFIA) biosensor has received wide-ranging interest in environmental monitoring and food analysis, as it provides the unique advantages of portability, simplicity and rapidity as well as low-cost equipment [1,2]. LFIA is mainly based on a specific reaction between probe (signal labeled antibody) and analytes, after analysis colored single or double lines could be formed by the accumulation of signal labels. As a signal provider, signal labels can directly affect the expression and sensitivity of LFIA biosensors. Conventionally, GNPs are used in LFIAs as signal labels owing to their good bioaffinity, easy synthesis and unique plasmon absorption [3]. Nevertheless, GNPs are often greatly limited by low sensitivity, chemical instability and high material consumption, which are not conducive to their further applications [4]. To overcome these situations, some novel nanomaterials were developed in LFIAs. Fluorescent nanomaterials, such as up-conversion nanomaterials (UCNPs) [5], quantum dots (QDs) [6] and semiconducting polymer dots [7] were applied due to their excellent fluorescence signal. But these fluorescent nanomaterials require complicated operations, advanced equipment and an extra excitation light, which greatly restrict the development of rapid detection. The exploitation of carbon-based nanomaterials for LFIA is a good adhibition of signal labels [8]. However, the large particle size of these carbon-based materials like carbon nanotube [9] and graphene [10] not only decreases the flow rate but also hinder the contaction and reaction between antibody and antigen, leading to a low sensitivity [11]. For instance, reduced graphene oxide at above 1000 nm was used as a signal label to detect *Escherichia coli O157:H7*, in this report, the immunoassay flow time arrived at 20 min, which dramatically extended the detecting time [12]. In addition, such large particles often make against smooth flow through nitrocellulose membrane pores and result in higher background signals due to nonspecific blockages.

Co_3O_4 nanoparticles (NPs), as a kind of promising transition metal oxide, have aroused a dramatic interest owing to its simple synthesis, low cost, good chemical stability and biocompatibility, which makes it remarkably be applied in various fields [13,14]. Meanwhile, benefiting from the unique control structure of rich morphology and different particle sizes ranging from tens to hundreds of nanometers [15,16], Co_3O_4 NPs have advantages in reducing steric hindrance and increasing the probability of immunological recognition. Additionally, Co_3O_4 NP is a classical cobalt-based black pigment with an intense brown color which can meet the requirement of signal labels in immunoassays [17]. To the best of our knowledge, the introduction of Co_3O_4 NPs as signal labels in the LFIA has not been investigated. Based on these above

* Corresponding author.
E-mail address: zhangdh@nwsuaf.edu.cn (D. Zhang).

https://doi.org/10.1016/j.talanta.2020.120729
Received 10 October 2019; Received in revised form 1 January 2020; Accepted 7 January 2020
Available online 08 January 2020
0039-9140/

superior characteristics, we can envisage Co_3O_4 NPs as an excellent signal label, which enables the LFIA platform to come out high sensitive, convenient and on-site detection in food safety mornitoring.

Furazolidone (FZD) is one of the broad spectrum antibiotics, which has been generally used to treat intestinal infection caused by *Escherichia coli* and *Salmonella spp* [18]. FZD is rapidly metabolized in animals and has a short half-life, but its metabolite AOZ can bind to cell membrane proteins in the body and remain for weeks [19]. Hence, the residual level of FZD is usually determined by using its metabolite AOZ as a target analyte. In this work, we synthesized dimercaptosuccinic acid (DMSA) modified Co_3O_4 NPs with high water solubility as signal labels to construct a novel LFIA biosensor for simple and rapid detection of AOZ. In order to verify the performance of this biosensor, traditional GNPs based LFIA was used for a comparison. In addition, this biosensor was applied in different real samples including honey, chicken, pork and milk powder to validate its feasibility. The established novel Co_3O_4 NPs-LFIA displayed high anti-interference ability, accuracy and sensitivity. This work proves that the small size Co_3O_4 NPs have great application potential as signal material in the lateral flow immunoassay for small molecule analytes.

2. Experimental

2.1. Materials and instrument

$Co(CH_3COO)_2{\cdot}4H_2O$ (Cobaltous acetate tetrahydrate) and ammonium hydroxide were purchased from Sinopharm Chemical Reagent Co,. Ltd (Beijing, China). AOZ, 3-[(4-carboxyphenyl) monomethyl] amino-2-oxazolidinone (CPAOZ), 1-aminohydantoin (CPAHD) semicarbazide (CPSEM), 3-amino-5-morpholinomethyl-2-oxazolidinone (CPAMOZ), penicillin and chloramphenicol were purchased from Anti Biotechnology (Wuhan, China). Hydrogen tetrachloroaurate (III) hydrate ($HAuCl_4{\cdot}3H_2O$) was purchased from Sigma-Aldrich (St. Louis, USA). Dimercaptosuccinic acid (DMSA) and dimethylsulfoxide (DMSO) were purchased form Aladdin chemistry Co. Ltd. (Shanghai, China). Anti-CPAOZ monoclonal antibody (mAb) was prepared in our lab (College of Food Science and Engineering, Northwest A & F University, Rapid monitoring laboratory for food safety). Goat anti-mouse immunoglobulin (IgG) was purchased from Luoyang Baiaotong Experimental Materials Center (Luoyang, China). Nitrocellulose (NC) membranes were purchased from Millipore Corp (Shanghai, China). Glass fibers, absorbent pads and polyvinyl chloride plate were received from Shanghai Kingdiag-biotech Co,. Ltd (Shanghai, China). Honey, milk powder, pork and chicken were obtained from a supermarket in Yangling, China. Other reagents include ethanol, hydrochloric acid, nitric acid, and sodium hydroxide were purchased from Aladdin chemistry Co. Ltd. (Shanghai, China). All other chemicals in this work were of analytical grade or higher.

Guillotine cutter (HGS-201) and Dispensing Platform (HGS510-2D) were received from Hangzhou Autokun Technology Co., Ltd (Hangzhou, China). Transmission electron microscopy (TEM) image was recorded by a JEOL JEM-1230 (Tokyo, Japan). The X-ray diffraction (XRD) pattern of Co_3O_4 NPs was performed on a Bruker D8 Advanced X-ray Diffractometer, equipped with Cu Kα radiation (Karlsruhe, Germany). An X-ray photoelectron spectroscopy (XPS) spectrum was conducted by Axis Ultra DLD X-ray photoelectron spectrometer (Shimadzu, England). The fourier-transform infrared (FT-IR) spectra were performed with a Vetex 70 (Bruker Corp, Germany). The zeta potentials of Co_3O_4 NPs and Co_3O_4 NPs-mAb solutions were measured using Zetasizer Nano-ZS instrument (Malvern, UK). All pH measurements were displayed with a PB-10 digital pH-meter (Sartorius, Germany).

2.2. Synthesis of the Co_3O_4 NPs and GNPs

Co_3O_4 NPs were synthesized using a hydrothermal method with minor modifications [16,20]. Briefly, 0.5 g of $Co(CH_3COO)_2{\cdot}4H_2O$ was dissolved into the mixed solvent containing 10 mL of deionized water and 15 mL of ethanol. Then, 2.5 mL of 25% ammonia was added to the above solution under vigorous stirring for 20 min. Afterward, the mixture was sealed into a Teflon-lined autoclave and heated at 150 °C for 3 h. The black products were collected by centrifugation and washed with water several times, followed by drying under vacuum at 60 °C. The dried Co_3O_4 NPs (20 mg) was dissolved into 50 mL water and adjusted pH to 2–3 by HCl (0.1 M). Following that, 1 mg DMSA was dissolved in 1 mL DMSO, and then quickly injected into the Co_3O_4 NPs solution under stirring. After the mixture was ultrasonic for 2 h and stirred for another 5 h, the product was collected with centrifugation and washed with water several times. The final product was stored at 4 °C for subsequent measurement.

GNPs were prepared by the citrate reduction process [21]. Briefly, all glassware was soaked in aqua royal (HCL: HNO_3 = 3 : 1) for 2 h and rinsed with water. 1 mL 1% (w/v) $HAuCl_4{\cdot}3H_2O$ solution was injected into 96 mL deionized water and heated until boiling under vigorous stirring. Then, 3 mL 1% (w/v) trisodium citrate was quickly added to the mixed solution, which gave rise to the solution changes from yellowish green to red. The solution was stirred for 15 min after the color change, cooled to ambient temperature and stored in refrigerator at 4 °C.

2.3. Preparation of the Co_3O_4 NPs-mAb and GNPs-mAb probes

Co_3O_4 NPs (1 mg) was dissolved into 1 mL borate buffer (2 mM, pH 7.4), soon afterward 3 μg (1 mg mL^{-1}) anti-CPAOZ mAb was added into the mixture with stirring for 2 h. Then, the mixture was blocked by 100 μL 10% BSA under stirring for another 30 min and washed three times to remove excess reagent. The final precipitate Co_3O_4 NPs-mAb probes were suspended in 200 μL borate buffer.

Initially, 1.0 mL of GNPs solution was adjusted pH to 8.0–9.0 by addition of 0.1 M K_2CO_3. The 4 μg anti-CPAOZ mAb was introduced to pH adjusted GNPs solution and incubated for 30 min at room temperature. Then, 10% BSA was injected into the mixture to obtain final 1% BSA concentration and incubated for another 30 min to block the residual active sites of GNPs. After incubation for 2 h at 4 °C, the solution was centrifuged at 1500 rpm for 15 min to remove unreactive anti-CPAOZ mAb and BSA. The precipitate was washed two times with 2 mM borax buffer (pH 9.0) containing 0.02% sodium azide (NaN_3) and 0.1% (w/v) PEG-20000 and separated by centrifugation at 12,000 rpm for 35 min. Finally, the GNPs-mAb probes were suspended in 100 μL borate buffer and stored at 4 °C for following use.

2.4. Fabrication of the Co_3O_4 NPs-LFIA

As shown in Scheme 1, the lateral flow strip was composed of 5 parts: absorbent pad, NC membrane, sample pad, conjugate pad and substrate plate. Both conjugate pad and sample pad were pretreated with blocking buffer and dried at 37 °C. The test line (T line) and control line (C line) were separately prepared by dispensing 0.3 mg mL^{-1} antigen (CPAOZ-BSA) and 0.5 mg mL^{-1} goat anti-mouse IgG solutions on the NC membrane. The distance between T and C lines was 3 mm. After drying at 37 °C for 30 min, the NC membrane, sample pad, conjugate pad and absorbent pad were assembled on the substrate plate with a 1–2 mm overlap. The assembled plate was cut into individual 3 mm strips and stored at 4 °C.

2.5. Assay procedure of the Co_3O_4 NPs-LFIA

A series CPAOZ standard solution of different concentrations were diluted with phosphate buffered saline (PBS). The 100 μL standard solution containing 3 μL Co_3O_4 NPs-mAb probes or 4 μL GNPs-mAb probes was added onto the sample pad and migrated onward to the whole strip under the force of capillary action (n = 3). After 6 min, the result was observed by naked eyes as colorimetric and semi-

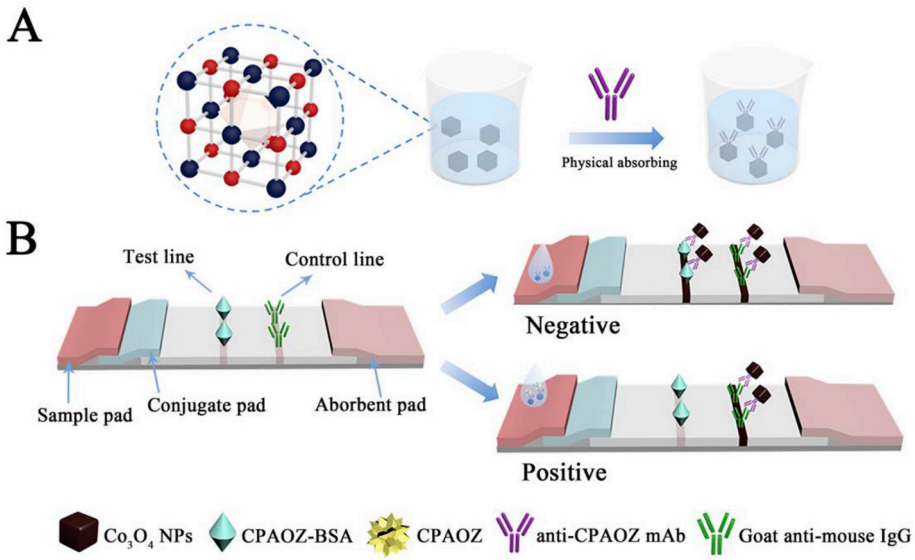

Scheme 1. (A) Coupling process of Co_3O_4 NPs with anti-CPAOZ mAbs; (B) Principle illustration of CPAOZ detection using the Co_3O_4 NPs-LFIA biosensor.

quantitative readouts. Afterward, the image was captured with a camera and the color intensities of T and C lines were processed with ImageJ software.

To evaluate the specificity of the Co_3O_4 NPs-LFIA, 10 ng mL^{-1} CPAOZ and 100 ng mL^{-1} of other structurally similar compounds (CPAHD, CPAMOZ, CPSEM, chloramphenicol and penicillin) were tested, respectively. PBS buffer solution was used as the control group. Each experiment was performed at least three times under the same operation.

2.6. AOZ detection in real samples by the Co_3O_4 NPs-LFIA

To verify the practicability of this Co_3O_4 NPs-LFIA, honey, milk powder, pork and chicken were selected as practical samples. This four food samples were previously confirmed to be nonexistent of AOZ by high performance liquid chromatography (HPLC). A simple pre-treatment of four samples was conducted using previously reported method with slight modifications [22]. The samples (1.0 g each) were added into disposable plastic centrifuge tubes and dissolved into water. Concretely, four samples were spiked with AOZ of different concentrations (0.2, 0.4, 0.8, 1, 2, 3 and 4 ng mL^{-1}) and sonication for 10 min. Subsequently, 200 μL of 0.05 M 4-nitrobenzaldehyde (4-CBA) in dimethyl sulfoxide (DMSO) was added to the above solutions and incubated at 37 °C for 16 h. The supernatant was then collected by centrifugation at 10,000 rpm for 10 min and analyzed by the prepared test strip under the optimal conditions.

3. Results and discussion

3.1. Principle of the Co_3O_4 NPs-LFIA

A novel Co_3O_4 NPs-LFIA biosensor was proposed and its design principle was displayed in Scheme 1. To greatly refrain from antibody denaturation and inactivation, the Co_3O_4 NPs were conjugated with anti-CPAOZ mAb by simple physical adsorption to form Co_3O_4 NPs-mAb probes (Scheme 1A). In the immunoassay, owing to the chromatography function the sample solution rapidly migrates from sample pad to absorbent pad along the strip forming colored bands on test zone. The detection of CPAOZ is based on a competitive format and the concentration of target CPAOZ is opposite to the color intensity of T line. As illustrated in Scheme 1B, if there exists no CPAOZ in the sample solution, the Co_3O_4 NPs-mAb probes would be captured by complete antigen of CPAOZ-BSA to form a distinct brown band. However, if CPAOZ is present, the competitive binding toward Co_3O_4 NPs-mAb probes will generate between the immobilized CPAOZ-BSA and target free CPAOZ, so that the color of T line will be shallower. When the CPAOZ content of sample is high enough, the reaction of CPAOZ-BSA and Co_3O_4 NPs-mAb probes will be completely blocked, and no color can be seen on the T line. No matter whether target CPAOZ is present in the sample solution, C line always shows color to ensure the validity of the LFIA.

3.2. Characterization of the Co_3O_4 NPs and Co_3O_4 NPs-mAb probes

The morphology and size of synthesized Co_3O_4 NPs were characterized by TEM. As shown in Fig. 1A, the resultant Co_3O_4 NPs exhibited a cubic shape and relatively homogeneous size distribution with an average diameter of 13.4 nm (determined by the measurement of 50 particles). The crystal structure and purity of Co_3O_4 NPs were also supported by XRD record. In Fig. 1B, the XRD pattern of Co_3O_4 NPs revealed peaks at 31.08°, 36.92°, 44.84°, 59.45° and 65.35° attributed to the (220), (311), (400), (511) and (440) reflection [23], which was coincided well with the standard XRD patterns of cubic spinel type Co_3O_4 NPs (JCPDS PDF 76–1802). As displayed in Fig. 1C, the FTIR spectrum of Co_3O_4 NPs had two distinctive absorption bands at 657 and 575 cm^{-1} assigned to Co–O stretching vibrations. The peak centered at 3429 and 1639 cm^{-1} separately corresponded to the –OH and O–H stretching vibrations of water molecules [24]. XPS was further measured to get the surface chemical composition and chemical states of Co_3O_4 NPs. As shown in Fig. S1A, the full survey scan spectrum of Co_3O_4 NPs can be indexed to Co 2p, O 1s and C 1s regions, which indicated that no other metallic elements or inorganic materials were involved in the results. Fig. S1B showed two major binding energies at 780.14 and 790.05 eV corresponding to Co $2p_{3/2}$ and Co $2p_{1/2}$, respectively. The two peaks of Co $2p_{3/2}$ located at 781.34 and 779.99 eV were characteristic of Co^{2+} and Co^{3+}, respectively [25]. These results indicated the successful synthesis of Co_3O_4 NPs in this work. Zeta potentials of the Co_3O_4 NPs and Co_3O_4 NPs-mAb were analyzed by dispersing them into deionized water. The change of zeta potential from −45.8 to −26.3 mV verified that the anti-CPAOZ mAb was successfully immobilized on the surface of Co_3O_4 NPs (Fig. 1D) [26].

3.3. Optimization of the Co_3O_4 NPs-LFIA

To obtain better immunoassay performances, the amount of anti-CPAOZ mAb, the volume of Co_3O_4 NPs-mAb and detection time were

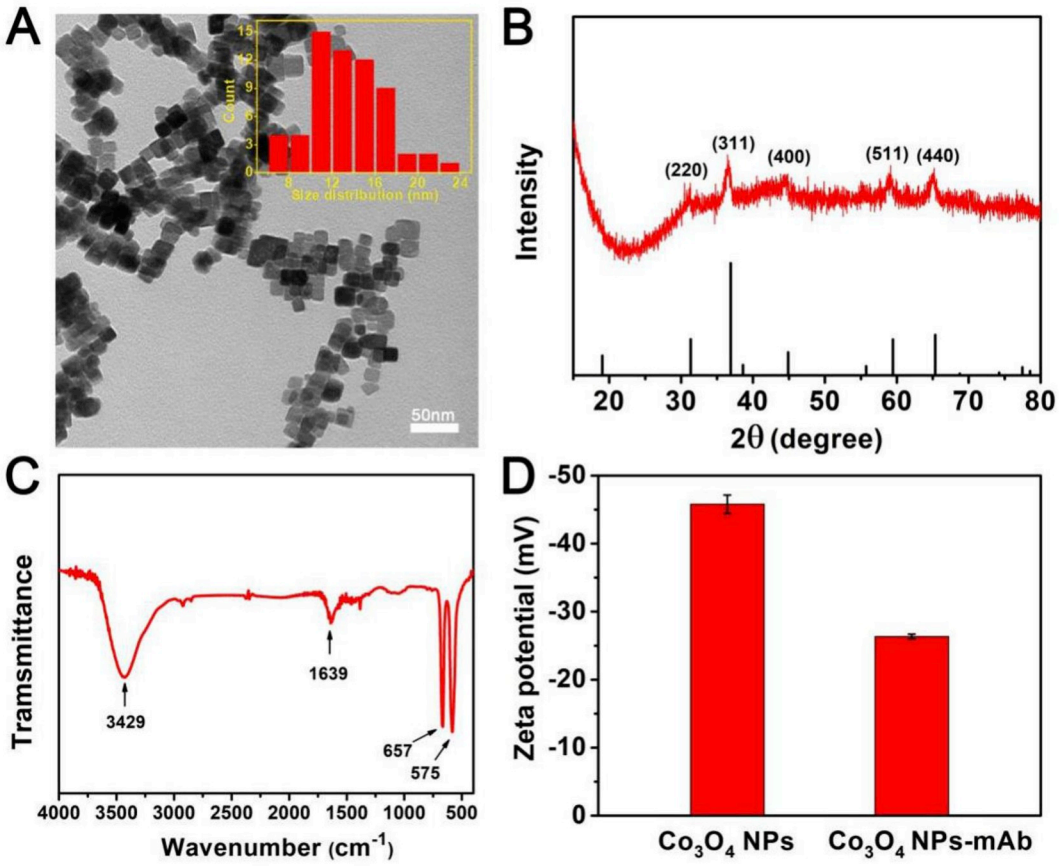

Fig. 1. (A) TEM image of Co_3O_4 NPs. The inset represents the corresponding nanoparticles size distribution histogram; (B) XRD pattern of Co_3O_4 NPs (red line) and standard Co_3O_4 NPs (JCPDS PDF 76–1802); (C) FTIR spectra of Co_3O_4 NPs; (D) Zeta potentials of Co_3O_4 NPs and Co_3O_4 NPs-mAb. (For interpretation of the references to color in this figure legend, the reader is referred to the Web version of this article.)

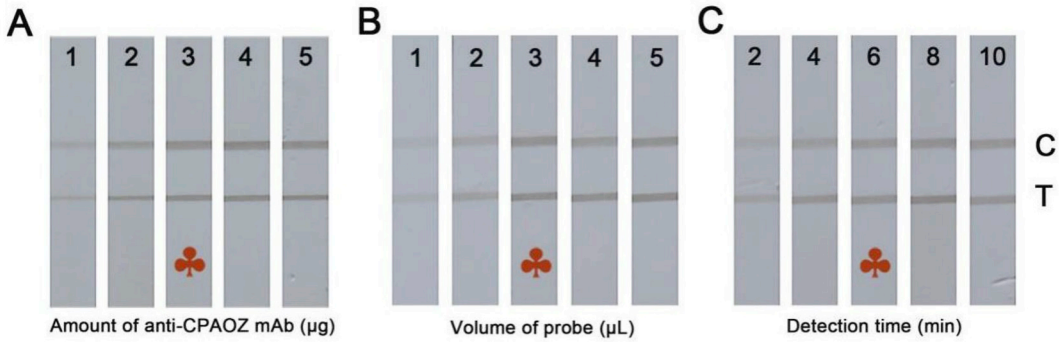

Fig. 2. Optimization results of experimental parameters of the Co_3O_4 NPs-LFIA. (A) Amount of anti-CPAOZ mAb (μg); (B) Volume of Co_3O_4 NPs-mAb probe; (C) Detection time. "T" stands for test line, "C" stands for control line and "♣" stands for the selected optimum condition.

optimized. The amount of anti-CPAOZ mAb was a crucial parameter that could affect the assay sensitivity for competitive immunoassay. To obtain the optimal amount of antibody binding on Co_3O_4 NPs, different amounts (1 μg, 2 μg, 3 μg, 4 μg and 5 μg) of anti-CPAOZ mAb were added into 1 mg mL^{-1} Co_3O_4 NPs solution, respectively. As displayed in Fig. 2A, the color intensities of T line and C line enhanced with increasing amount of anti-CPAOZ mAb at the range of 1–3 μg. An excess of antibodies might affect the competitive reaction and result in lower sensitivity. Considering from this aspect, 3 μg was sufficient and selected as the optimal amount of anti-CPAOZ mAb.

Moreover, as a recognition probe, Co_3O_4 NPs-mAb would selectively capture CPAOZ, and accumulate on the T line and C line to form brown bands for quantitative analysis. So, the volume of immunoassay probes could directly influence the color intensity and assay sensitivity. Fig. 2B shows the dependence of color intensity on volumes of probes in this assay system. When the volume of immunoassay probes increased to 3 μL, the test zone showed two distinct brown bands with a maximum color intensity. To avoid the inhibition of excessive probes toward the competitive reaction between immobilized antigens and target free molecules, 3 μL was chosen as the best volume of probes for the following measurement.

In order to realize rapid detection on spot, different detection time of the Co_3O_4 NPs-LFIA was investigated. As presented in Fig. 2C, the intensity of brown bands on both T line and C line gradually increased from 2 to 6 min and maintained a balance after 6 min. As shown in Fig. S3, between 3 repetitions, the optical density of T line demonstrates a

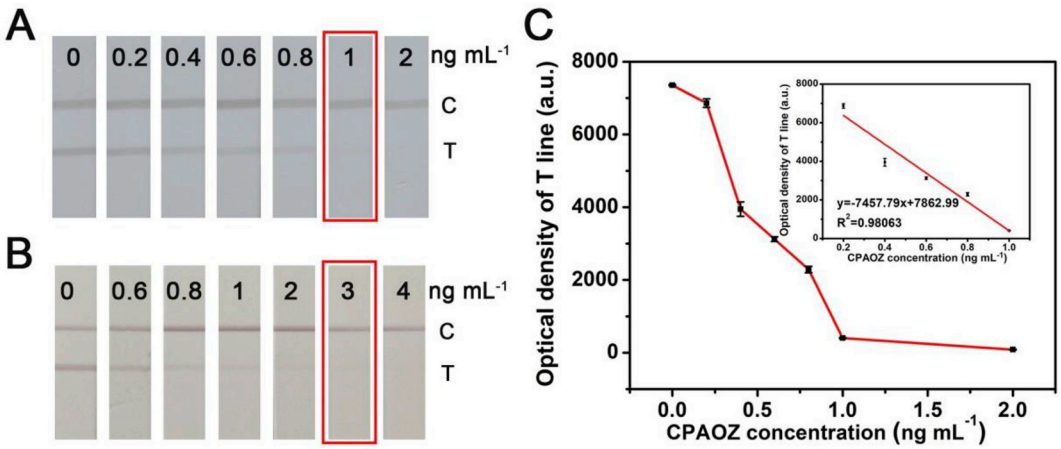

Fig. 3. (A) Results of CPAOZ detection by the Co_3O_4 NPs-LFIA; (B) Results of CPAOZ detection by the GNPs-LFIA; (C) The variation rule in the whole detection range of CPAOZ by the Co_3O_4 NPs-LFIA (inset image: calibration curve of CPAOZ). The error bars show the standard deviation of three replicates.

minimal error bar under the detection time of 6 min compared to other detection times, indicating the best repeatability for the observation of results at this time. While, the detection time is 8 min for the GNP-LFIA under best repeatability. Thus, in the following experiments 6 min was selected as the final detection time which was much faster than that of the conventional GNPs-LFIA. In addition, to achieve higher sensitivity of the Co_3O_4 NPs-LFIA as well as bright visual color bands on the strip, concentrations and dispensing rates of the CPAOZ-BSA and goat anti-mouse IgG in T and C lines, blocking buffers for sample and conjugate pads were also optimized. The optimal results were showed in Table S1.

Table 1
Performance comparison of the LFIAs for determination of FZD.

Labels	Detection limit (ng mL^{-1})	Readout mode	Detection time	Reference
Quantum dot	10	Naked eye	10 min	[27]
GNPs	10	Naked eye	10 min	[28]
Crystal violet	7	Naked eye	10 min	[29]
Co_3O_4 NPs	1	Naked eye	6 min	This work

3.4. Analytical performance of the Co_3O_4 NPs-LFIA

Under the optimized conditions, the sensitivity of the Co_3O_4 NPs-LFIA was evaluated with a range of CPAOZ standard solutions. The minimum target CPAOZ concentration of color vanishing on T line was set as the visual detection limit (VDL). As shown in Fig. 3A, with the gradually increasing of CPAOZ concentration, the color intensity of T line was reduced by degrees since a competitive inhibition effect of CPAOZ and complete antigen toward immune probes. When the concentration of CPAOZ reached 0.4 ng mL^{-1}, the color intensity of T line was significantly weaker than that on the negative strip by visual inspection, and the color intensity of T line almost completely disappeared at 1 ng mL^{-1} of CPAOZ. Thus, 1 ng mL^{-1} of CPAOZ was regarded as the VDL of the Co_3O_4 NPs-LFIA. Furthermore, quantitative analysis was realized by processing the gray value of color band on T line using ImageJ software. As shown in the inset of Fig. 3C, the corresponding calibration plots of optical density on T line had a great linear correlation (R^2 = 0.98,063) with the CPAOZ concentration in the range of 0.2–1 ng mL^{-1}. According to the following formula, the concentration of AOZ was converted from CPAOZ concentration.

$$C_{AOZ} = \frac{M_{AOZ}}{M_{CPAOZ}} \times C_{CPAOZ}$$

Where C_{CPAOZ} is concentration of CPAOZ detected in the LFIA. M_{AOZ} and M_{CPAOZ} represent relative molecular mass of AOZ and CPAOZ. C_{AOZ} is concentration of AOZ and can be calculated according to the formula. Therefore, after calculation the VDL of AOZ was 0.4 ng mL^{-1}. For a comparison, GNPs were used as signal tags to detect CPAOZ under the optimized conditions (Fig. S4), and as can be seen in Fig. 3B, the VDL value of the GNPs-LFIA reached 3 ng mL^{-1} for CPAOZ (1.3 ng mL^{-1} for AOZ). So, the sensitivity of the Co_3O_4 NPs-LFIA is 3-fold better than that of the conventional GNPs-LFIA. Compared with methods reported in previous literatures for FZD detection (Table 1), the Co_3O_4 NPs-LFIA also displayed greater superiority, which could be mainly ascribed to the better biocompatibility and higher color depth of Co_3O_4 NPs. What's more, as signal labels, the small size of Co_3O_4 NPs obviously reduced the steric hindrance and accelerated the immune responses of antigen and antibody. Therefore, the Co_3O_4 NPs-LFIA can be applied as a promising platform for highly sensitive and rapid detection of FZD.

In addition, the specificity of the Co_3O_4 NPs-LFIA was investigated via testing several structural analogues including CPAHD, CPAMOZ, CPSEM, chloramphenicol and penicillin respectively at the same concentration of 100 ng mL^{-1}. As revealed in Fig. 4A, positive results were only seen in the presence of CPAOZ (10 ng mL^{-1}), while the color intensities of T line were almost the same as that of the negative control strip even at a high concentration for other structurally similar compounds. Meantime, the corresponding gray values of T line for all analytes were presented in Fig. 4B. As a result, the developed LFIA had no cross-reactivity with these similar-structure small molecules and could be used as a highly selective platform to detect CPAOZ.

In order to evaluate the precision of the Co_3O_4 NPs-LFIA, standardized recovery tests of AOZ toward blank milk powder have been carried out. Each addtion concentration was detected every 4 h for three times during the same day, and measured within seven days (1, 3, 7 day) to evaluate the within-day and between-days repeatability. As shown in Table S2, based on the method of Co_3O_4 NPs-LFIA, the relative standard deviation (RSD) values were all below 9.4%, and the recovery rates ranged from 98% to 105%, indicating good precision of this method.

3.5. Application in food samples of the Co_3O_4 NPs-LFIA

For a further evaluation of reliability and practicability of the Co_3O_4 NPs-LFIA, honey, chicken, pork, milk powder were selected as actual samples to detect AOZ via the standard addition method. After deriving the AOZ to CPAOZ (Fig. S2), the obtained sample solutions were tested by Co_3O_4 NPs-LFIA. As displayed in Fig. 5, the VDL of AOZ in honey, chicken and pork samples were all 3 ng mL^{-1}, and 1 ng mL^{-1} in milk

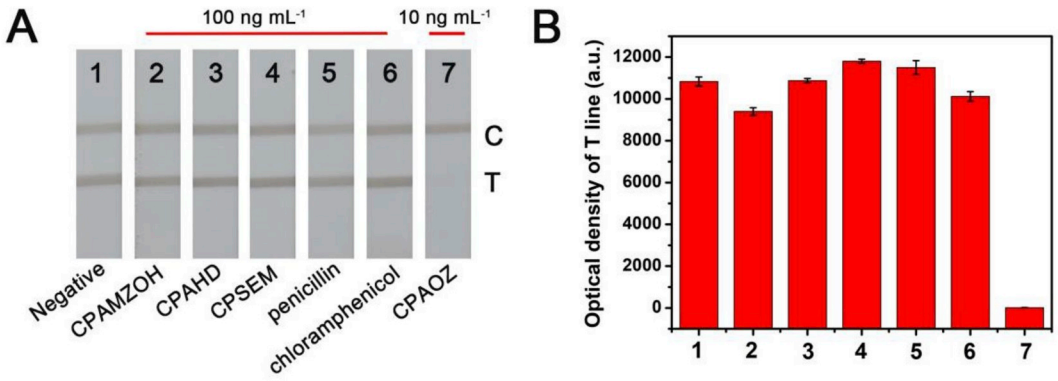

Fig. 4. (A)–(B) Specificity results of the Co_3O_4 NPs-LFIA. The concentration of CPAOZ is 10 ng mL^{-1}, concentrations of CPAMZOH, CPAHD, CPSEM, penicillin and chloramphenicol are all 100 ng mL^{-1}. The error bars show the standard deviation of three independent experiments.

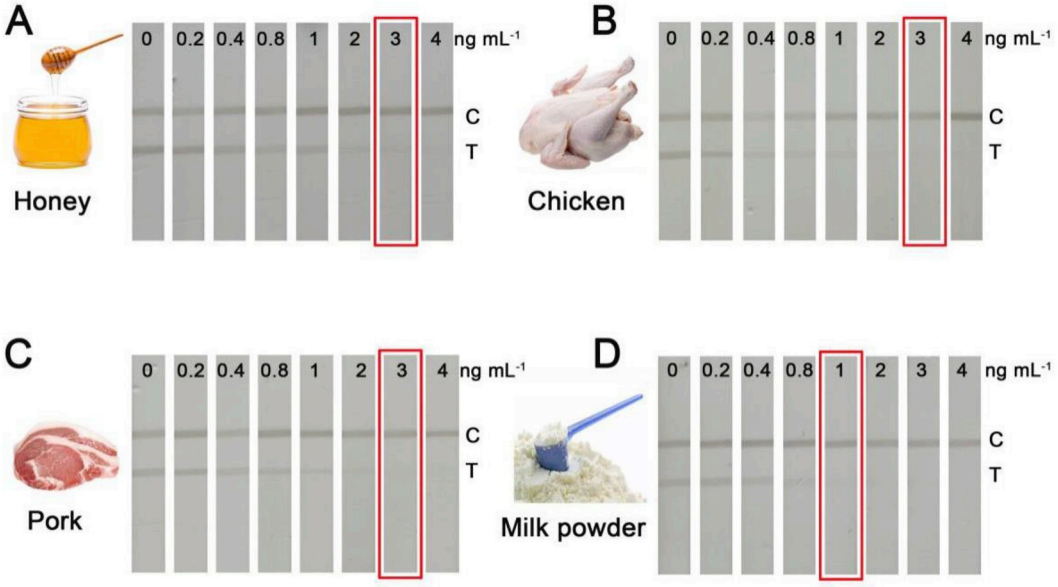

Fig. 5. Detection results of AOZ in honey (A), chicken (B), pork (C), milk powder (D) samples based on the Co_3O_4 NPs-LFIA.

powder. The analytical performance of this Co_3O_4 NPs-LFIA in the actual samples was decreased slightly compared with standard tests due to the food matrix interference. Even so, this biosensor provided great potential for its application in the real samples.

4. Conclusion

In summary, a highly efficient and sensitive Co_3O_4 NPs-LFIA biosensor was successfully developed to detect AOZ. Co_3O_4 NPs were proved to be able to applied as desired immunoassay signal labels owing to their simple synthesis and intense color. Compared with some other signal labels, the small size of Co_3O_4 NPs in this work possessed a great possible advantage in the aspects of distinctly reducing the steric hindrance and promoting the probability of immune recognition, which was beneficial for high assay sensitivity. Under optimal conditions, the developed Co_3O_4 NPs-LFIA displayed great selectivity and high sensitivity to AOZ with a detection limit of 0.4 ng mL^{-1} by naked eyes, which was 3-fold improvement than that of the conventional LFIA. Furthermore, this Co_3O_4 NPs-LFIA had great potential for detection of AOZ in different real samples. Owing to these superior advantages such as short detection time, simple equipment and high sensitivity, the proposed Co_3O_4 NPs-LFIA is expected to be widely applied in food safety and environmental monitoring.

Declaration of competing interest

We declare that we have no financial and personal relationships with other people or organizations that can inappropriately influence our work, there is no professional or other personal interest of any nature or kind in any product, service and/or company that could be construed as influencing the position presented in, or the review of, the manuscript entitled.

Acknowledgments

The authors thank the National Science Foundation of China (21675127, 31972150), the Shaanxi Provincial Science Fund for Distinguished Young Scholars (2018JC-011), the Key Research and Development Plan of Shaanxi Province (2019NY-109), Shaanxi Province characteristic industry innovation chain (2019ZDLSF07-08), the Development Project of Qinghai Provincial Key Laboratory (2017-ZJ-Y10), and the Capacity Building Project of Engineering Research Center of Qinghai Province (2017-GX-G03).

Appendix A. Supplementary data

Supplementary data to this article can be found online at https://doi.org/10.1016/j.talanta.2020.120729.

References

[1] M.J. Raeisossadati, N.M. Danesh, F. Borna, M. Gholamzad, M. Ramezani, K. Abnous, et al., Lateral flow based immunobiosensors for detection of food contaminants, Biosens. Bioelectron. 86 (2016) 235–246.

[2] X. Yao, Z. Wang, L. Dou, B. Zhao, Y. He, J. Wang, et al., An innovative immunochromatography assay for highly sensitive detection of 17β-estradiol based on an indirect probe strategy, Sens. Actuators B Chem. 289 (2019) 48–55.

[3] H. Aldewachi, T. Chalati, M.N. Woodroofe, N. Bricklebank, B. Sharrack, P. Gardiner, Gold nanoparticle-based colorimetric biosensors, Nanoscale 10 (2017) 18–33.

[4] J. Hu, Z.L. Zhang, C.Y. Wen, M. Tang, L.L. Wu, C. Liu, et al., Sensitive and quantitative detection of C-reaction protein based on immunofluorescent nanospheres coupled with lateral flow test strip, Anal. Chem. 88 (2016) 6577–6584.

[5] P. Wang, R. Wang, W. Zhang, X. Su, H. Luo, Novel fabrication of immunochromatographic assay based on up conversion phosphors for sensitive detection of clenbuterol, Biosens. Bioelectron. 77 (2016) 866–870.

[6] L. Guo, Y. Shao, H. Duan, W. Ma, Y. Leng, X. Huang, et al., Magnetic quantum dot nanobead-based fluorescent immunochromatographic assay for the highly sensitive detection of aflatoxin B1 in dark soy sauce, Anal. Chem. 91 (2019) 4727–4734.

[7] X. Gong, J. Cai, B. Zhang, Q. Zhao, J. Piao, W. Peng, et al., A review of fluorescent signal-based lateral flow immunochromatographic strips, J. Mater. Chem. B 5 (2017) 5079–5091.

[8] Z. Wang, X. Yao, R. Wang, Y. Ji, T. Yue, J. Sun, et al., Label-free strip sensor based on surface positively charged nitrogen-rich carbon nanoparticles for rapid detection of Salmonella enteritidis, Biosens. Bioelectron. 132 (2019) 360–367.

[9] Y. Huang, Y. Wen, K. Baryeh, S. Takalkar, M. Lund, X. Zhang, et al., Magnetized carbon nanotubes for visual detection of proteins directly in whole blood, Anal. Chim. Acta 993 (2017) 79–86.

[10] L. Yu, P. Li, X. Ding, Q. Zhang, Graphene oxide and carboxylated graphene oxide: viable two-dimensional nanolabels for lateral flow immunoassays, Talanta 165 (2017) 167–175.

[11] Y. Zhou, L. Ding, Y. Wu, X. Huang, W. Lai, Y. Xiong, Emerging strategies to develop sensitive AuNP-based ICTS nanosensors, Trac. Trends Anal. Chem. 112 (2019) 147–160.

[12] V. Shirshahi, S.N. Tabatabaei, S. Hatamie, R. Saber, Functionalized reduced graphene oxide as a lateral flow immuneassay label for one-step detection of Escherichia coli O157:H7, J. Pharm. Biomed. Anal. 164 (2019) 104–111.

[13] W. Qin, L. Su, C. Yang, Y. Ma, H. Zhang, X. Chen, Colorimetric detection of sulfite in foods by a TMB-O2-Co3O4 nanoparticles detection system, J. Agric. Food Chem. 62 (2014) 5827–5834.

[14] X. Zhou, Z. Liu, Y. Wang, Y. Ding, Facet effect of Co 3 O 4 nanocrystals on visible-light driven water oxidation, Appl. Catal. B Environ. 237 (2018) 74–84.

[15] J. Feng, H.C. Zeng, Size-controlled growth of Co3O4Nanocubes, Chem. Mater. 15 (2003) 2829–2835.

[16] J. Mu, L. Zhang, M. Zhao, Y. Wang, Catalase mimic property of Co3O4 nanomaterials with different morphology and its application as a calcium sensor, ACS Appl. Mater. Interfaces 6 (2014) 7090–7098.

[17] E. Lester, G. Aksomaityte, J. Li, S. Gomez, J. Gonzalez-Gonzalez, M. Poliakoff, Controlled continuous hydrothermal synthesis of cobalt oxide (Co3O4) nanoparticles, Prog. Cryst. Growth Charact. Mater. 58 (2012) 3–13.

[18] X. Lu, X. Liang, J. Dong, Z. Fang, L. Zeng, Lateral flow biosensor for multiplex detection of nitrofuran metabolites based on functionalized magnetic beads, Anal. Bioanal. Chem. 408 (2016) 6703–6709.

[19] C. Xing, X. Jing, X. Zhang, J. Yuan, Ultrasensitive indirect competitive ELISA and strip sensor for detection of furazolidone metabolite in animal tissues, Food Agric. Immunol. 28 (2017) 1269–1282.

[20] P. Wang, L. Cao, Y. Chen, Y. Wu, J. Di, Photoelectrochemical biosensor based on Co3O4 nanoenzyme coupled with PbS quantum dots for hydrogen peroxide detection, ACS Applied Nano Materials 2 (2019) 2204–2211.

[21] D.H. Choi, S.K. Lee, Y.K. Oh, B.W. Bae, S.D. Lee, S. Kim, et al., A dual gold nanoparticle conjugate-based lateral flow assay (LFA) method for the analysis of troponin I, Biosens. Bioelectron. 25 (2010) 1999–2002.

[22] L. Yan, L. Dou, T. Bu, Q. Huang, R. Wang, Q. Yang, et al., Highly sensitive furazolidone monitoring in milk by a signal amplified lateral flow assay based on magnetite nanoparticles labeled dual-probe, Food Chem. 261 (2018) 131–138.

[23] Q. Jiao, M. Fu, C. You, Y. Zhao, H. Li, Preparation of hollow Co3O4 microspheres and their ethanol sensing properties, Inorg. Chem. 51 (2012) 11513–11520.

[24] T. Wang, J. Wang, Y. Yang, P. Su, Y. Yang, Co3O4/Reduced graphene oxide nanocomposites as effective phosphotriesterase mimetics for degradation and detection of paraoxon, Ind. Eng. Chem. Res. 56 (2017) 9762–9769.

[25] L. Li, Q. Yang, C. Zhang, J. Yan, Y. Peng, J. Li, Hollow-structural Ag/Co3O4 nanocatalyst for CO oxidation: interfacial synergistic effect, ACS Applied Nano Materials 2 (2019) 3480–3489.

[26] T. Yang, C.M. Li, J.H. He, B. Chen, Y.F. Li, C.Z. Huang, Ratiometrically fluorescent electrospun nanofibrous film as a Cu(2+)-mediated solid-phase immunoassay platform for biomarkers, Anal. Chem. 90 (2018) 9966–9974.

[27] T. Le, Y. Xie, L. Zhu, L. Zhang, Rapid and sensitive detection of 3-Amino-2-oxazolidinone using a quantum dot-based immunochromatographic fluorescent biosensor, J. Agric. Food Chem. 64 (2016) 8678–8683.

[28] Y. Xie, L. Zhang, T. Le, An immunochromatography test strip for rapid, quantitative and sensitive detection of furazolidone metabolite, 3-amino-2-oxazolidinone, in animal tissues, Food Agric. Immunol. 28 (2017) 403–413.

[29] L. Dou, T. Bu, W. Zhang, B. Zhao, Q. Yang, L. Huang, et al., Chemical-staining based lateral flow immunoassay: a nanomaterials-free and ultra-simple tool for a small molecule detection, Sens. Actuators B Chem. 279 (2019) 427–432.